

RESEARCH ARTICLE

10.1002/2017TC004519

Seismic anisotropy and mantle dynamics beneath the Malawi Rift Zone, East Africa

Cory A. Reed¹ , Kelly H. Liu¹ , Youqiang Yu^{1,2} , and Stephen S. Gao^{1,3} ¹Geology and Geophysics Program, Missouri University of Science and Technology, Rolla, Missouri, USA, ²State Key Laboratory of Marine Geology, Tongji University, Shanghai, China, ³College of Earth Science, Northeast Petroleum University, Daqing, China

Key Points:

- The first shear wave splitting study of the Malawi Rift Zone reveals mantle anisotropy consistent with no-net rotation absolute plate motion models
- Anisotropy develops in the transitional layer between the lithosphere and asthenosphere, and mantle flow is deflected by edges of thick lithosphere
- No upwelling or small-scale convection flow beneath this young continental rift, suggesting an upper mantle origin of rift initiation and early development

Supporting Information:

- Supporting Information S1
- Table S1
- Table S2

Correspondence to:

S. S. Gao,
sgao@mst.edu

Citation:

Reed, C. A., K. H. Liu, Y. Yu, and S. S. Gao (2017), Seismic anisotropy and mantle dynamics beneath the Malawi Rift Zone, East Africa, *Tectonics*, 36, 1338–1351, doi:10.1002/2017TC004519.

Received 18 FEB 2017

Accepted 12 JUN 2017

Accepted article online 22 JUN 2017

Published online 22 JUL 2017

Abstract SKS, SKKS, and PKS splitting parameters measured at 34 seismic stations that we deployed in the vicinity of the Cenozoic Malawi Rift Zone (MRZ) of the East African Rift System demonstrate systematic spatial variations with an average splitting time of 1.0 ± 0.3 s. The overall NE-SW fast orientations are consistent with absolute plate motion (APM) models of the African Plate constructed under the assumption of no-net rotation of the global lithosphere and are inconsistent with predicted APM directions from models employing a fixed hot spot reference frame. They also depart considerably from the trend of most of the major tectonic features. These observations, together with the results of anisotropy depth estimation using the spatial coherency of the splitting parameters, suggest a mostly asthenospheric origin of the observed azimuthal anisotropy. The single-layered anisotropy observed at 30 and two-layered anisotropy observed at 4 of the 34 stations can be explained by APM-related simple shear within the rheologically transitional layer between the lithosphere and asthenosphere, as well as by the horizontal deflection of asthenospheric flow along the southern and western edges of a continental block with relatively thick lithosphere revealed by previous seismic tomography and receiver function investigations. This first regional-scale shear wave splitting investigation of the MRZ suggests the absence of rifting-related active mantle upwelling or small-scale mantle convection and supports a passive-rifting process for the MRZ.

1. Introduction

The Malawi Rift Zone (MRZ) initiated at ~ 8.6 Ma with the synchronous onset of volcanism in the Rungwe Volcanic Province at its northern terminus [Ebinger *et al.*, 1989, 1993]. The Mbeya triple junction located at the northern edge of the volcanic province acts as the nexus of the Nubian plate and the Victoria and Rovuma microplates [Delvaux *et al.*, 1992] (Figure 1). The spreading rate of the MRZ decreases progressively toward the south [Calais *et al.*, 2006], and the Rovuma Microplate is separating from the Nubian Plate along a rift-perpendicular direction at rates of 2.2 mm/yr and 0.8 mm/yr at the northern and southern tips of the MRZ, respectively [Saria *et al.*, 2014]. Unlike most other segments in the Cenozoic East African Rift System (EARS) and the Permo-Triassic Luangwa Rift Zone (LRZ), which largely developed in ancient orogenic belts that wrap around the edges of relatively strong continental blocks [Chorowicz, 2005], the ~ 800 km long, N-S oriented MRZ traverses a complicated set of Precambrian crustal terranes separated by suture or shear zones with a variety of orientations and is not following known preexisting orogenic belts [Craig *et al.*, 2011; Fritz *et al.*, 2013; Laó-Dávila *et al.*, 2015]. Accordingly, the initiation and evolution of this young continental rift are puzzling [Huerta *et al.*, 2009; Stamps *et al.*, 2014] and have attracted numerous geoscientific investigations including two recent large-scale interdisciplinary studies [Gao *et al.*, 2013; Shillington *et al.*, 2016].

One of the major seismological techniques frequently used to delineate mantle structure and dynamics is shear wave splitting (SWS) analysis [e.g., Ando *et al.*, 1980; Silver and Chan, 1991; Gao *et al.*, 1994, 1997, 2010; Yu *et al.*, 2015], which measures seismic azimuthal anisotropy that is quantified by two splitting parameters, including the polarization orientation of the fast wave (ϕ or fast orientation which is measured clockwise from north) and the time separation between the fast and slow waves (δt or splitting time) which has a global average of 1.0 s [Silver, 1996]. The most commonly employed seismic phases for SWS analysis are *P*-to-*S* converted phases at the core-mantle boundary on the receiver side, including PKS, SKKS, and SKS (hereafter collectively referred to as XKS) [Silver and Chan, 1991].

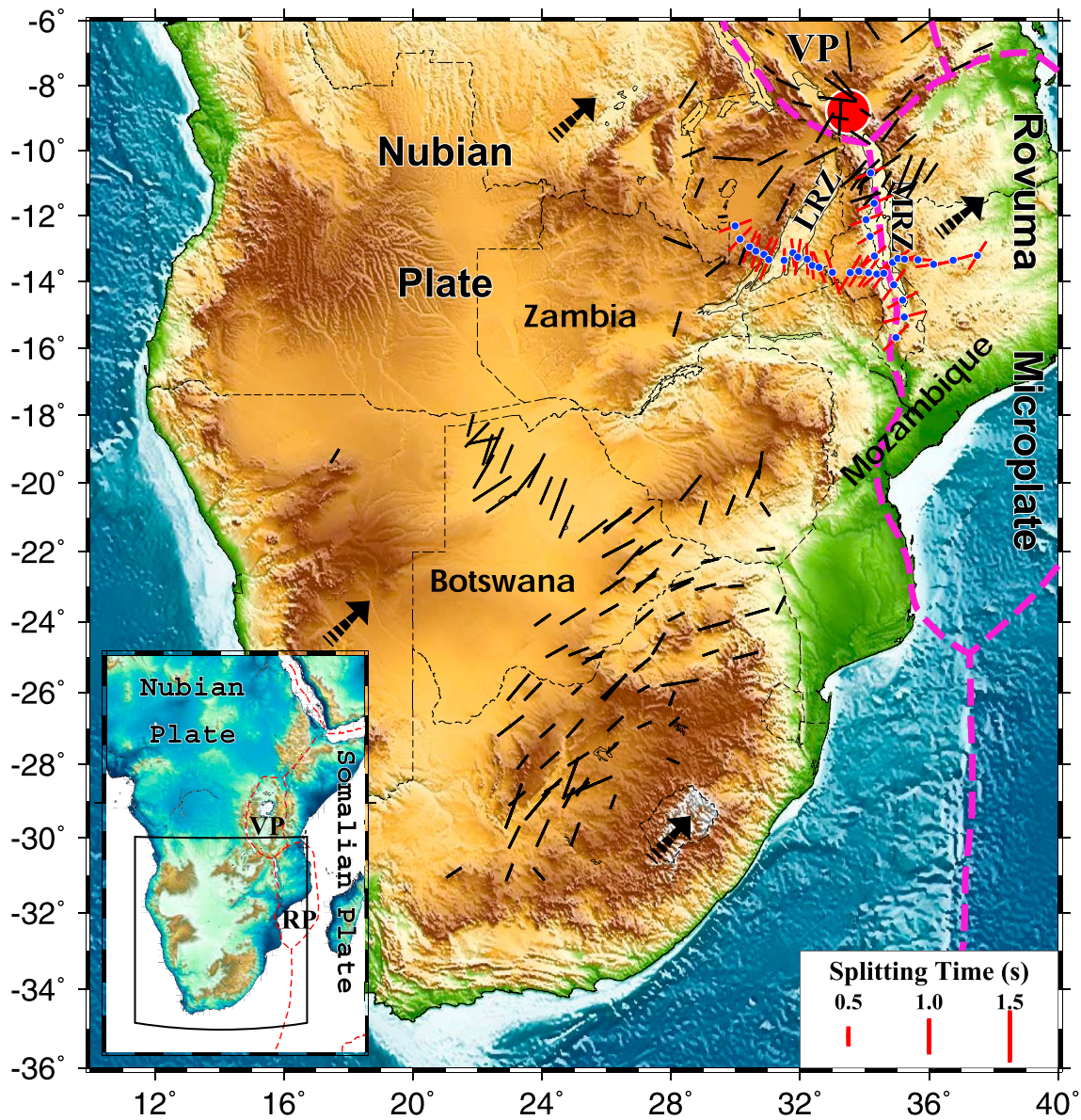


Figure 1. A digital elevation map of southern Africa demonstrating station-averaged shear wave splitting parameters produced by previous studies (black bars) [Barruol and Ben Ismail, 2001; Silver *et al.*, 2001; Walker *et al.*, 2004; Bagley and Nyblade, 2013; Yu *et al.*, 2015; Tepp, 2016] and this study (red bars). Thick dashed magenta lines delineate plate boundaries from Stamps *et al.* [2008], and black arrows indicate the APM of the African Plate according to NNR-MORVEL56 [Argus *et al.*, 2011]. The red circle represents the Mbeya triple junction. MRZ, Malawi Rift Zone; LRZ, Luangwa Rift Zone. The inset shows the study area. VP, Victoria Microplate; RP, Rovuma Microplate.

Numerous processes in the Earth's interior are capable of generating measurable seismic azimuthal anisotropy [e.g., Silver, 1996; Savage, 1999; Long and Silver, 2009]. In the asthenosphere, the most commonly invoked mechanism for the formation of seismic anisotropy is the simple shear strain of olivine aggregates caused by the movement of the lithosphere relative to the underlying asthenosphere, a phenomenon which increases with plate age and relative velocity [Tommasi *et al.*, 1996]. This simple shear induces dislocation slip and a cumulative lattice-preferred orientation (LPO) that leads to observable azimuthal anisotropy with the fast orientation parallel to the flow direction [Zhang and Karato, 1995]. Orogenic sutures and regional-scale faults, both of which result in lithospheric vertically coherent deformation, can produce fast orientations that are subparallel to the strike of the mountain chain or fault zone [Silver *et al.*, 2001]. In areas such as continental rifts that are dominated by extensional stresses, melt pockets and dikes in the lithosphere can lead to rift-parallel fast orientations [Gao *et al.*, 1997, 2010; Hammond *et al.*, 2014].

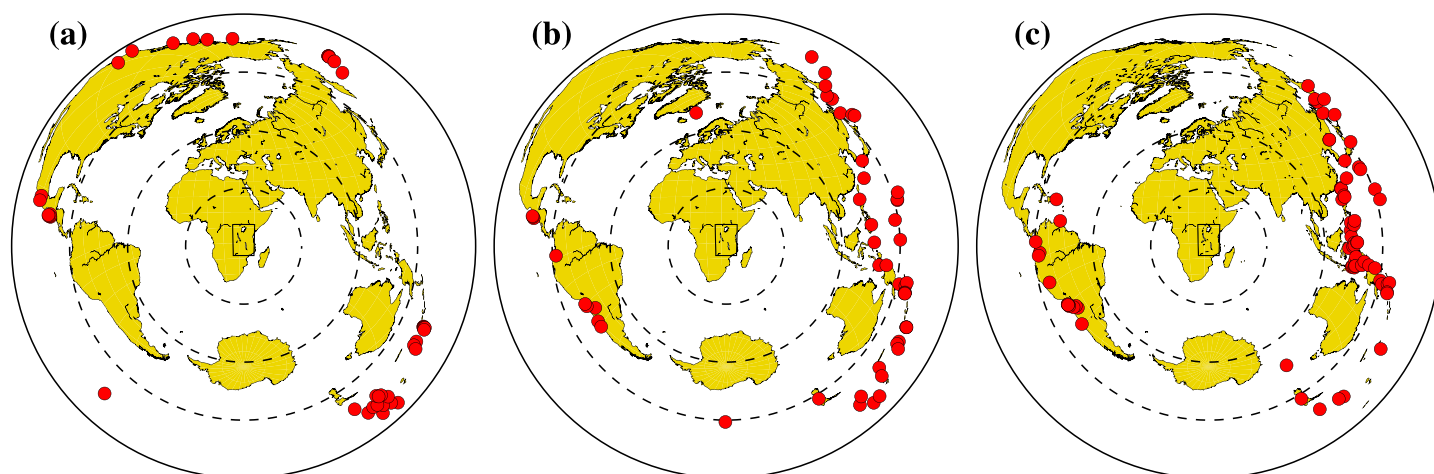


Figure 2. Azimuthal equidistant maps showing the spatial distribution of the (a) 42 PKS, (b) 51 SKKS, and (c) 73 SKS events that yielded at least one rank A or B measurement in this study.

SWS observations in southern and eastern Africa have been reported by a number of groups using different measuring techniques and data processing parameters (Figure 1) [Gao *et al.*, 1997; Barruol and Ben Ismail, 2001; Silver *et al.*, 2001; Walker *et al.*, 2004; Bagley and Nyblade, 2013; Yu *et al.*, 2015; Tepp, 2016]. The majority of the ϕ measurements in southern and eastern Africa are NE-SW (Figure 1) with localized variations. With the exception of the northern tip of the MRZ, the vast extent of the young rift has not been investigated using SWS analysis. Here we provide SWS measurements using recently recorded broadband seismic data along two profiles to quantify the orientation, strength, and layering of seismic anisotropy beneath the MRZ and adjacent areas and to provide new constraints on mantle flow and rifting models.

2. Data and Methods

This study employs broadband seismic data recorded by 34 stations that we deployed in Malawi, Mozambique, and Zambia over a 2 year period from June 2012 to June 2014 (Figure 1 and Table S1 in the supporting information). The stations belong to the SAFARI (Seismic Arrays For African Rift Initiation) experiment [Gao *et al.*, 2013; Reed *et al.*, 2016] (network code XK). Fifteen stations were situated in Malawi, seven in Mozambique, and 12 in Zambia along an ~ 900 km E-W and an ~ 600 km N-S array (Figure 1). The stations are named by a five-character string, with the first letter denoting the country name (Q for Mozambique, W for Malawi, and Z for Zambia). It is followed by two digits that represent the station number within the country. The last two letters represent the geographic location. If a station was moved to a different location, its new name retains the first three characters, while the final two letters reflect the new site.

The epicentral distance of the events used in the study is $120\text{--}180^\circ$ for PKS, $95\text{--}180^\circ$ for SKKS, and $84\text{--}180^\circ$ for SKS, respectively [Liu and Gao, 2013]. The cutoff magnitude is 5.6 for events with focal depths shallower than 100 km and 5.5 for deeper events (Figure 2). The XKS waveforms are band-pass filtered using a Butterworth four-pole two-pass filter with corner frequencies of 0.04 and 0.5 Hz, and events with an XKS signal-to-noise ratio (SNR) less than 4.0 on the radial component are discarded. The optimal splitting parameters (ϕ and δt) for each event-station pair are subsequently grid searched using the procedure outlined in Liu and Gao [2013], which seeks to minimize the XKS energy on the corrected transverse component [Silver and Chan, 1991]. The XKS window used for the grid search is initially set to 5 s before and 20 s following the predicted IASP91 arrival of the XKS phase.

Manual screening of each individual measurement is conducted to verify the reliability, as is indicated by the SNR of both the original radial and transverse components, the goodness of matching between the fast and slow components, the linearity of the corrected particle motion, the completeness of the removal of the XKS energy on the corrected transverse component, the strength and uniqueness of the energy minimum on the contour plot of the corrected energy, and the magnitude of the errors of the resulting parameters. If necessary,

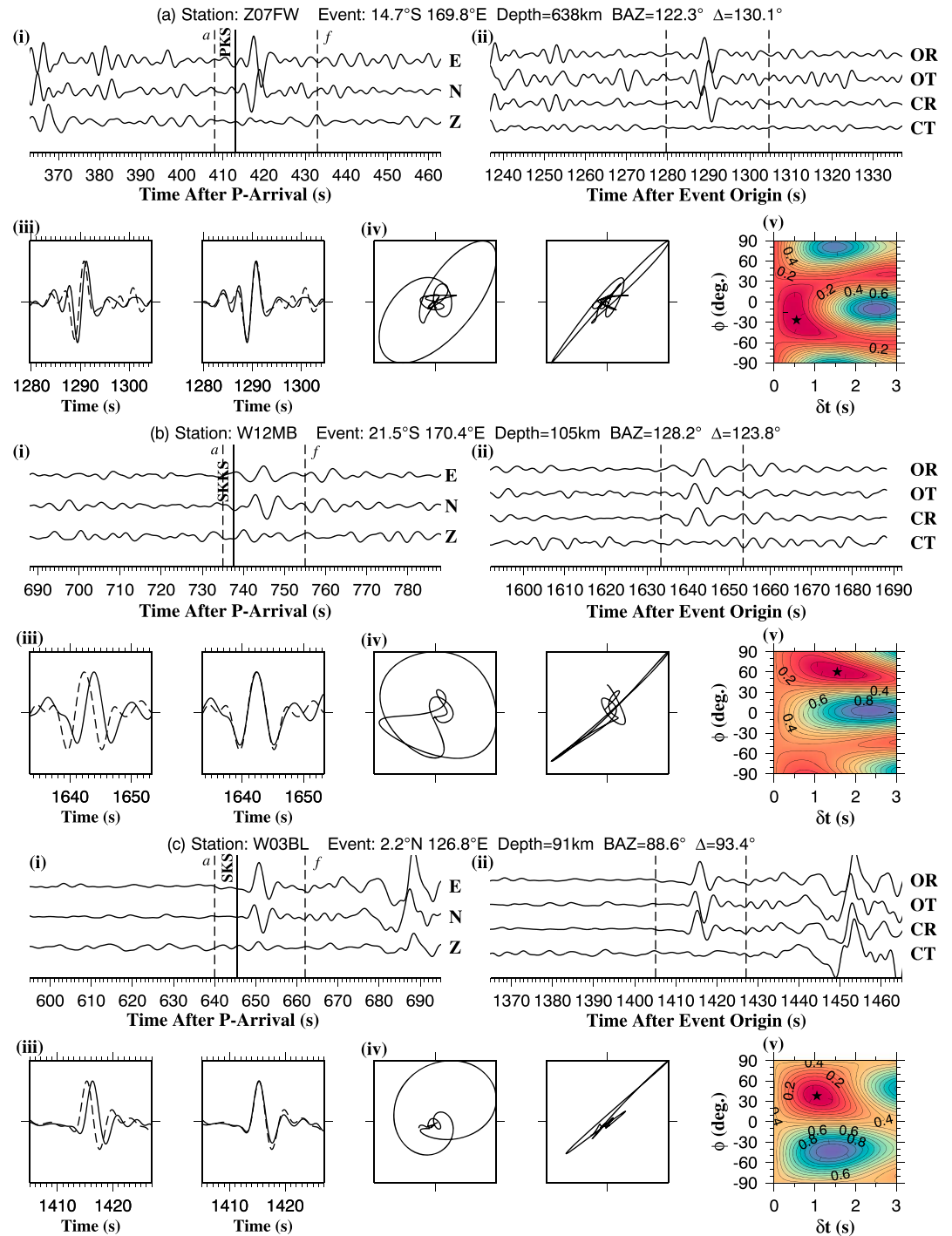


Figure 3. (a) Examples of PKS, (b) SKKS, and (c) SKS splitting measurements. For each XKS phase, (i) original E-N-Z components, (ii) original and corrected radial and transverse components, (iii) fast (dashed) and slow (solid) components, (iv) original (left) and corrected (right) horizontal particle motion, and (v) contour of corrected transverse energy with the optimal pair of splitting parameters corresponding to the minimum transverse energy (black star).

modifications are made to the boundaries of the time window and the band-pass filter frequencies to improve the above indicators. Rankings are initially assigned based upon the SNR of the original and corrected radial and transverse components and are manually verified and, if necessary, adjusted accordingly. The rankings include A (outstanding), B (good), C (poor), and N (null). Details of the ranking procedure are provided

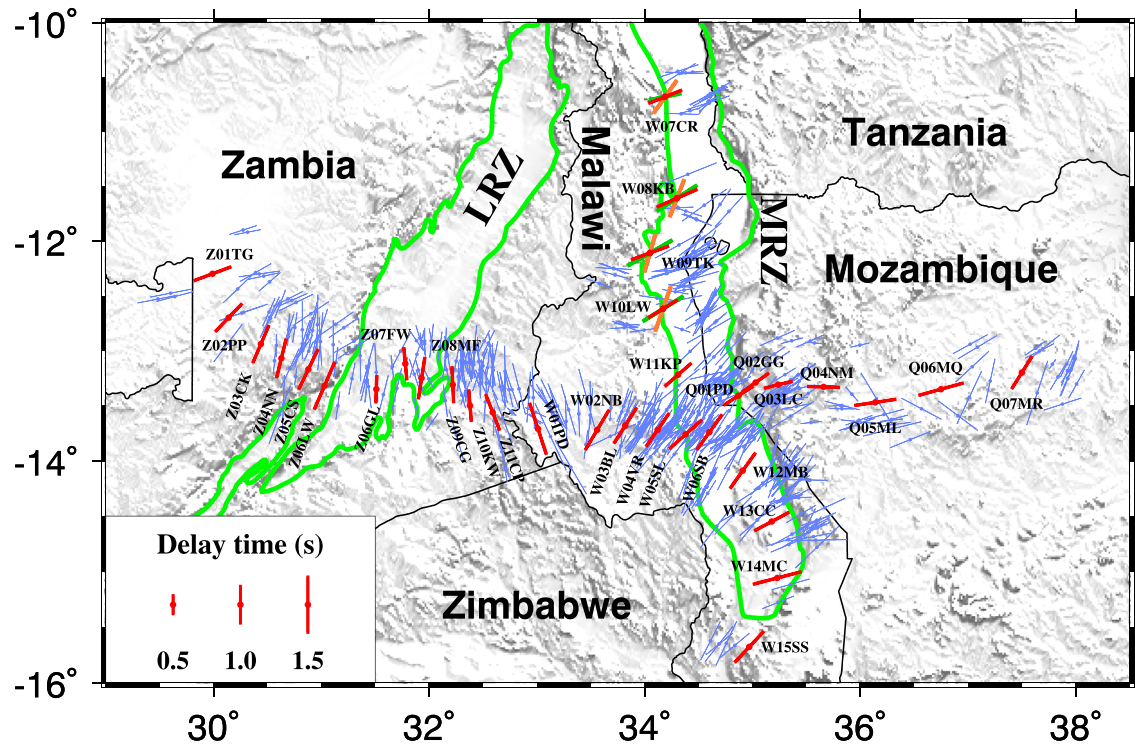


Figure 4. Station-averaged (thick red bars) and individual (thin purple bars) SWS measurements plotted at the stations and above the ray-piercing points at 200 km depth, respectively. For the four northernmost stations, results of two-layer fitting are also plotted, with the orange bars representing the parameters for the lower layer and the green bars for the upper layer. The areas outlined by the green lines are the Luangwa and Malawi rift zones.

in Liu *et al.* [2008], and examples for the three XKS phases are shown in Figure 3 (plots similar to Figure 3 for all the 538 event-station pairs can be found in the rightmost column of <http://www.mst.edu/%7Esgao/MalawiSWS>, while the leftmost column shows the individual measurements plotted against the back azimuth of the events).

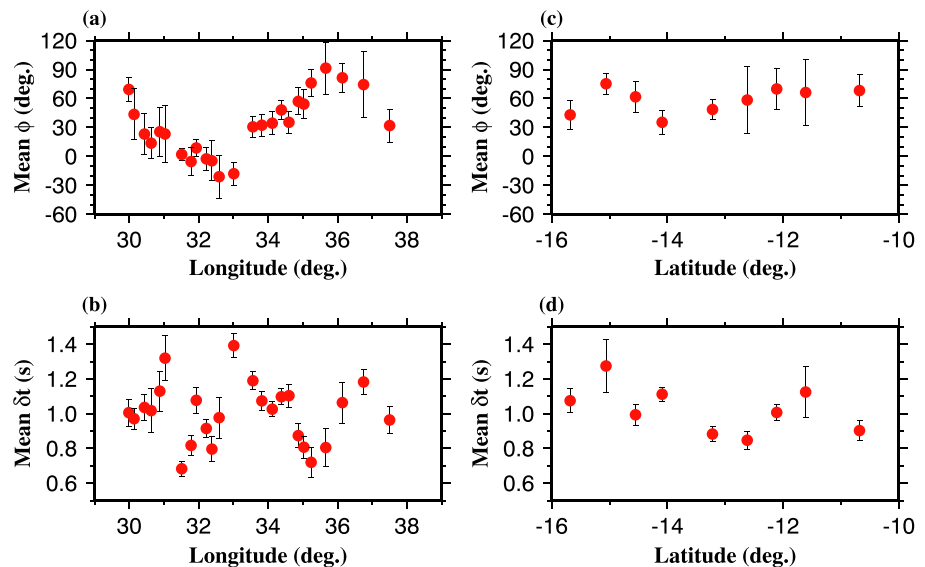


Figure 5. Station-averaged (a, c) fast orientations and (b, d) splitting times along the E-W (Figures 5a and 5b) and N-S (Figures 5c and 5d) profiles computed using well-defined splitting measurements.

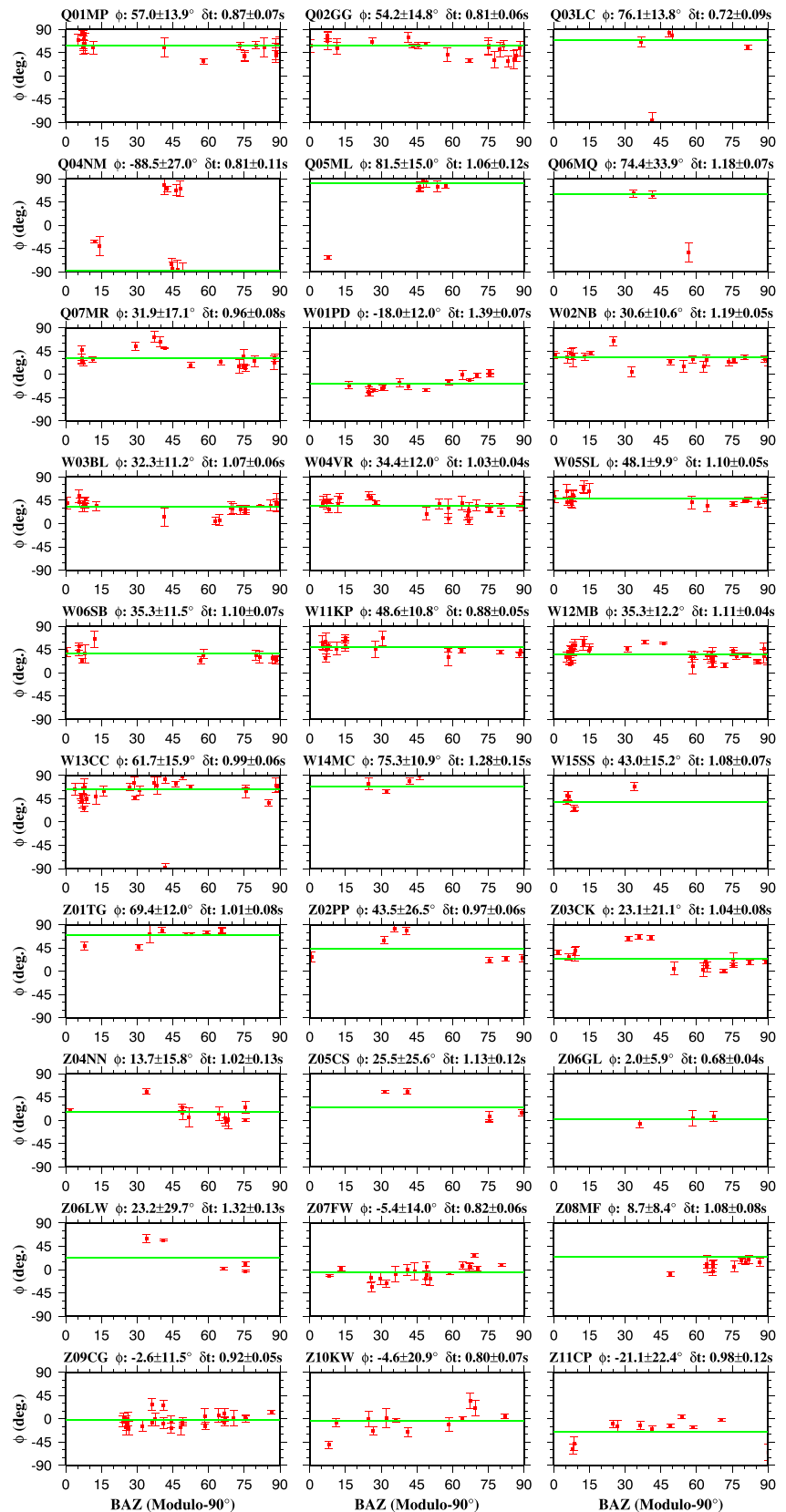


Figure 6. Fast orientations plotted against the modulo-90° BAZ for each of the 30 stations showing insignificant periodic azimuthal variations of the fast orientations. The green bar in each of the plots shows the station-averaged value.

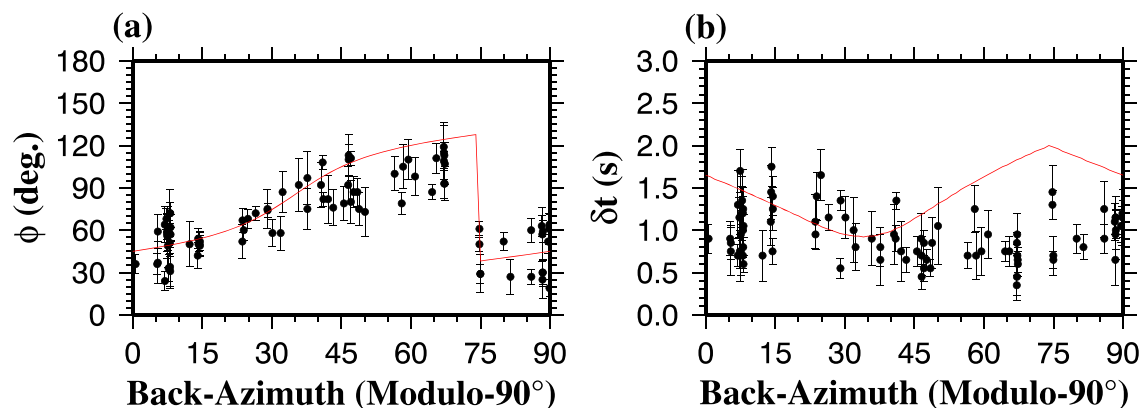


Figure 7. Observed splitting parameters at the four stations in the northern MRZ (dots) and theoretical splitting parameters (red lines) computed using the results of grid searching under a two-layered model ($\phi=27^\circ$ and $\delta t=1.5$ s for the lower layer, and $\phi=69^\circ$ and $\delta t=1.0$ s for the upper layer). (a) Fast orientations, and (b) splitting times.

3. Results

A total of 538 quality A or B measurements are obtained at 34 stations, including 81 PKS, 139 SKKS, and 318 SKS measurements (Figure 4 and Table S1). Due to the fact that nonnull measurements are observed for all of the stations that recorded a reliable XKS signal, null measurements are not reported because they reflect either the situation wherein the back azimuth (BAZ) of the event is parallel to the fast or slow orientation, or when the XKS energy on the original transverse component is too weak relative to the noise, and thus is unable to be observed visually [Liu and Gao, 2013]. Station-averaged fast orientations are calculated as the circular mean of the individual ϕ measurements from the station, and station-averaged splitting times are the simple mean of the individual δt measurements (Figure 4 and Table S2). The circular mean of all 538 ϕ measurements is $39 \pm 32^\circ$, and the mean δt is 1.0 ± 0.3 s. Figure 5 shows the station-averaged splitting parameters plotted along both the E-W and N-S profiles.

To investigate the existence of 90° periodic azimuthal variations of the resulting splitting parameters against the BAZ, which is a diagnostic feature of two-layered anisotropic structure with a horizontal axis of symmetry [Silver and Savage, 1994], we plot the splitting parameters against the modulo- 90° of the BAZ, i.e., $BAZ_{90} = BAZ - 90(n - 1)$ where $n = 1, 2, 3, 4$ is the quadrant number (Figures 6 and 7), as well as against the BAZ (Figure 8). Figures 7 and 8 show that a clear 90° azimuthal periodicity exists for four of the 34 stations. All the four stations are located in the northern MRZ and have a similar pattern of azimuthal variation (Figures 7 and 8). Due to the limited back-azimuthal range, the existence of periodic azimuthal variation for several stations shown in Figure 6 (e.g., Q05ML, W06MQ, W15SS, and Z06GL) cannot be definitively determined. These stations are categorized as single-layered based on the similarity of the splitting parameters with neighboring stations in the single-layered group.

3.1. Rift-Orthogonal Profile

Significant and systematic spatial variations of the station-averaged splitting parameters are detected across the E-W array (Figures 5a and 5b). An approximately 90° counterclockwise progressive rotation of ϕ is observed among the stations west of 33° E, ranging from about 70° at the westernmost station (Z01TG) to about -20° at station W01PD (Figures 4 and 5). The fast orientations then establish a 50° clockwise shift, producing a dominantly NE-SW orientation at station W02NB. The value of ϕ gradually rotates clockwise toward the east and becomes approximately E-W at most of the stations in Mozambique (Figures 4 and 5). The variation of the splitting times along the profile is less systematic, although stations with a NE-SW fast orientation generally have larger-than-normal splitting times, while those with a more E-W fast orientation have the smallest splitting times (Figures 5a and 5b). The mean splitting parameters for measurements along the rift-orthogonal profile are $37 \pm 34^\circ$ for ϕ and 0.99 ± 0.30 s for δt .

3.2. Rift-Parallel Profile

The splitting parameters observed at the four stations situated in the northern MRZ exhibit systematic azimuthal variations with a 90° periodicity (Figures 7 and 8). The station-averaged ϕ values at these stations are NE-SW, which is similar to the average over all of the 34 stations, but they possess large standard errors

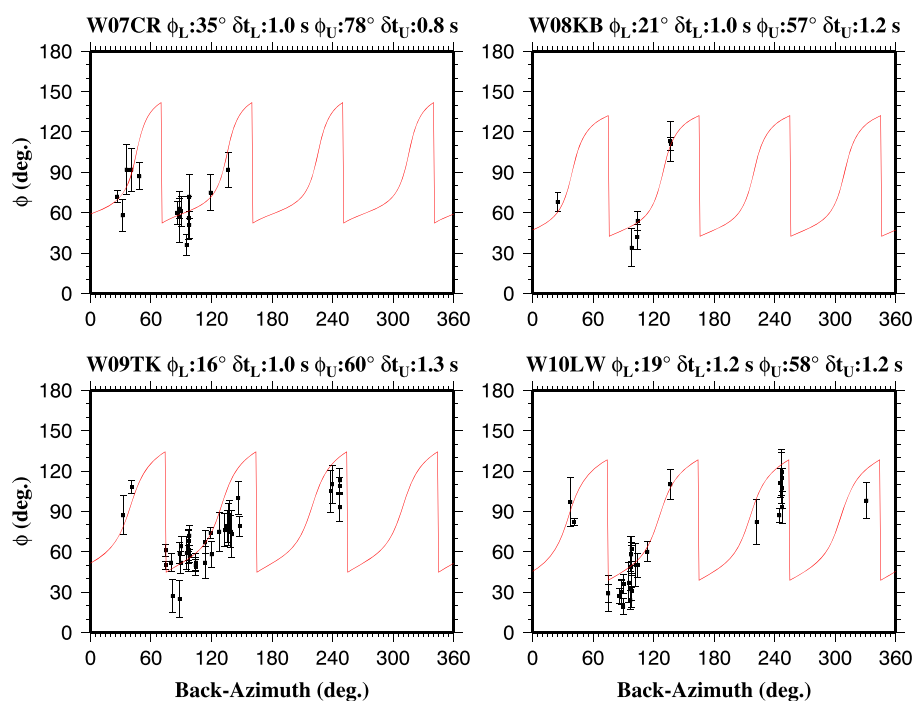


Figure 8. Azimuthal variation of individual ϕ measurements for each of the four northern MRZ stations. The best fitting two-layer parameters are shown at the top of each plot, and the red curves are theoretical ϕ values calculated using the best fitting parameters.

due to their azimuthal variations (Figure 5c). The maximum difference in ϕ among the individual events is 56° for W07CR, 79° for W08KB, 88° for W09TK, and 80° for W10LW. The rest of the stations in the rift-parallel profile are characterized by a prevalent NE-SW station-averaged fast orientation, which is everywhere oblique to the MRZ rift axis. The delay time from these 10 stations exhibits no discernible pattern relative to the southward decreasing spreading rate of the MRZ [Saria *et al.*, 2014]. The mean δt along this profile is 1.00 ± 0.30 s, which is identical to the global average [Silver, 1996], and the mean ϕ is $55 \pm 24^\circ$.

We next attempt to fit the azimuthal variation of the splitting parameters observed at the four northern MRZ stations under a two-layered model with a horizontal axis of symmetry using the approach of Silver and Savage [1994]. In order to reduce the well-known nonuniqueness of the resulting two pairs of splitting parameters when measurements from individual stations are used, we take a two-step approach that is similar to what we have recently utilized to constrain the two-layered structure in Tian Shan [Cherie *et al.*, 2016]. For the first step, we combine measurements from the four stations and perform a grid search of the two pairs of the splitting parameters using a peak frequency of 0.25 Hz and weighting factors of 0.8 and 0.2 for ϕ and δt , respectively [Gao and Liu, 2009]. The resulting splitting parameters are 27° and 1.5 s for the lower layer, and 69° and 1.0 s for the upper layer. For the second step, the optimal splitting parameters for each of the layers are grid searched by using the above splitting parameters as constraints. Specifically, for the lower layer, the search range is -20° to 50° for ϕ , and 0.5–2.0 s for δt ; for the upper layer, the corresponding ranges are 0° to 90° and 0.5–2.0 s. The resulting two-layered model for each of the four stations is shown in Figure 8. The ϕ for the lower layer ranges from 16° to 35° and that for the upper layer ranges from 57° to 78° .

4. Discussion

4.1. Anisotropy Layer Depth Estimation

Due to the steep raypath of the XKS phases, the vertical resolution of the SWS technique is low. In this section, we estimate the depth of the center of the anisotropic layer by applying a method that utilizes the spatial coherency of splitting parameters [Gao and Liu, 2012; Liu and Gao, 2011] employing measurements from the 30 stations with data that are representative of simple anisotropy (Figure 6). The procedure dictates that the optimal depth of the anisotropic layer will correspond to the minimum spatial variation factor (F_v), which is a function of the sum of the weighted standard deviations (i.e., the variation factors) of both the ϕ and δt values

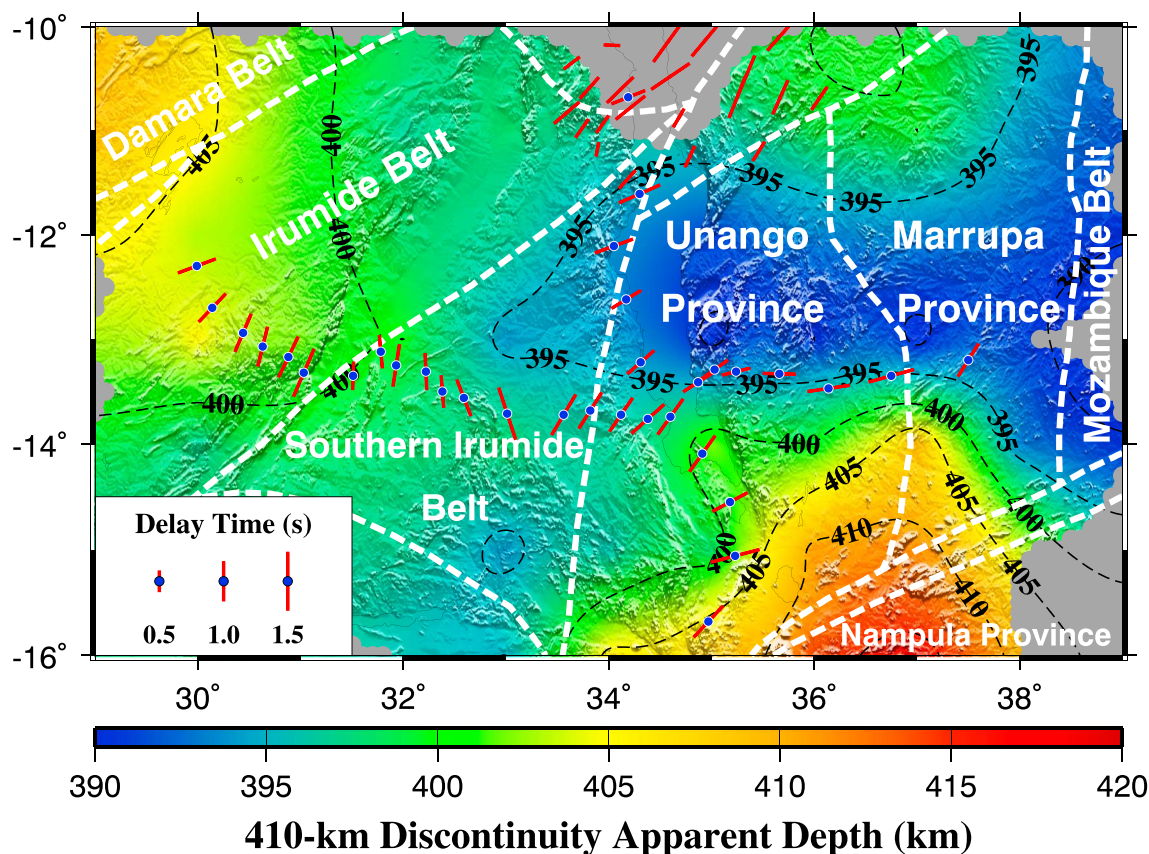


Figure 9. Contour of apparent depths of the 410-km discontinuity (black dashed lines) [Reed *et al.*, 2016] and station-averaged splitting parameters from this study (red bars with blue circles) and Tepp [2016] (red bars). Dashed white lines are major basement tectonic boundaries [Craig *et al.*, 2011].

that are averaged over moving geographic windows (see Liu and Gao [2011], for an expanded description and Gao and Liu [2012], for a detailed description of an open-access computer program). This technique requires a decent BAZ coverage, densely spaced (e.g., 70 km or less) stations and gradual lateral variations in the spatially varying simple anisotropy.

Similar to what has been utilized to estimate the depth of anisotropic layers elsewhere (e.g., Yang *et al.* [2017], for the eastern United States and Yu *et al.* [2015], for the Okavango Rift Zone), we conduct a search for the optimal depth of anisotropy within a vertical range from the surface to a depth of 400 km by computing the F_v for each depth at an incremental step of 5 km. We employ this technique using two different geographic window sizes: $0.25^\circ \times 0.25^\circ$ and $0.45^\circ \times 0.45^\circ$. These two window sizes are utilized in order to demonstrate the overall variability within the resulting output. A minimum of two well-defined splitting measurements are required within each window. The resulting optimal depths for the center of the layer of anisotropy beneath our study area are found to range between 220 and 265 km for window sizes of 0.25° and 0.45° , respectively (Figure S1). A similar determination of the depth of anisotropy using SWS measurements in the vicinity of the Okavango Rift Zone in Botswana [Yu *et al.*, 2015] uncovered an optimal depth between 240 and 280 km.

4.2. Relationship Between SWS and Major Geological Features

The 34 SAFARI stations employed in this study are situated within a network of major lithospheric shear zones and tectonic terranes [Craig *et al.*, 2011] (Figure 9). While some of the ϕ measurements are consistent with the local strike of the terrane boundaries, the vast majority are not. For instance, the structural trend of the major tectonic boundaries in northern Mozambique is predominantly N-S (Figure 9) and is thus inconsistent with the E-W fast orientations observed therein. In addition, with the exception of the several measurements near the western boundary of the LRZ, most of the measurements in the vicinity of the MRZ and LRZ are not parallel to the primary border faults which strike roughly parallel to the rifts (Figure 4) [Delvaux *et al.*, 1992; Banks *et al.*, 1995; Fritz *et al.*, 2013].

Another argument against a significant lithospheric contribution is that such a contribution, together with contributions from simple shear in the lithosphere-asthenosphere transitional layer described below, would form a two-layered anisotropic structure [Yang *et al.*, 2017]. This structure, unless the fast orientations of the two layers therein are the same or 90° apart, would lead to systematic azimuthal variations of the splitting parameters [Yang *et al.*, 2017]. Such variations are not observed at most of the stations (Figure 6). Finally, increases in the splitting times are not found near the terrane boundaries, which are locations of strain localization and should correspond to larger splitting times if lithospheric fabrics dominate.

Therefore, while contributions to the observed anisotropy from fossil fabrics related to past tectonic events cannot be completely ruled out, the inconsistencies between the observed fast orientations and the trend of major tectonic features, and the lack of systematic azimuthal variations of the splitting parameters observed at most of the stations (Figure 6), suggest that these contributions may not be sufficiently significant to account for most of the observed anisotropy. A possible exception for this is in the vicinity of the LRZ (Figure 4), where the parallelism between the fast orientations and the dominant strike of the western boundary of the LRZ may indicate strong frozen-in lithospheric fabrics. If this is true, an interesting question for future investigations is why preferably oriented lithospheric fabrics are preserved along some but not all ancient tectonic boundaries.

4.3. Relationship Between SWS and Models of Absolute Plate Motion

Many SWS observational and modeling studies attribute the observed azimuthal anisotropy to the simple shear strain associated with absolute plate motion (APM) models [e.g., Becker *et al.*, 2003, 2006; Liu *et al.*, 2014], and the most frequently utilized APM models are those constructed under the assumption of a fixed Pacific hot spot reference frame such as HS3-NUVEL-1A [Gripp and Gordon, 2002]. This attribution is primarily due to the fact that the majority of the observed fast orientations are subparallel to the predicted APM direction of the tectonic plates, such as the North American Plate [Fouch *et al.*, 2000; Becker *et al.*, 2006; Liu *et al.*, 2014; Yang *et al.*, 2017].

The correspondence between the observed fast orientations and those predicted by HS3-NUVEL-1A and other models with a westward net rotation (NR) of the lithosphere [e.g., Conrad and Behn, 2010], however, breaks down for the African Plate, where the predicted fast orientation is mostly E-W, while the observed fast orientations are N-S for northern Africa [Lemnifi *et al.*, 2015; Elsheikh *et al.*, 2014] and NE-SW for southern and eastern Africa (Figure 1) [Silver *et al.*, 2001; Yu *et al.*, 2015; Tepp, 2016]. Meanwhile, most no-net rotation (NNR) APM models [e.g., DeMets *et al.*, 1994; Argus *et al.*, 2011] as well as the surface-plate driven model of Conrad and Behn [2010] predict a NE-SW fast orientation for the study area that is consistent with the observed fast orientations (Figure 1).

These observations may suggest that at least in the vicinity of the MRZ and perhaps most of southern and eastern Africa, the net rotation of the lithosphere does not produce significant simple shear in the upper mantle, implying that the upper asthenosphere also has a westward net rotation of similar direction and speed. Under this hypothesis, the apparent correspondence between the observed fast orientations and the ones predicted using models with a net rotation component in some plates, such as North America, is the result of the fact that the plate motions in both the NNR and NR frames are similar or are 180° apart. Thus, at least for most part of Africa, NNR APM models such as NNR-MORVEL56 [Argus *et al.*, 2011] are better poised for comparison with SWS measurements relative to those developed under a fixed hot spot reference frame.

4.4. Lithospheric Modulation of Flow and APM-Induced Anisotropy

The absence of similarity between the observed fast orientations and the dominant strike of the major tectonic features in most of the study area (Figure 1), the results of the estimation of the anisotropic layer depth, as well as the overall consistency between the fast orientations and the APM direction suggest a primarily asthenospheric origin of the observed seismic anisotropy. While a variety of potential models may exist, the vast majority of the SWS observations can be explained by a simple model involving two deformation systems, as recently proposed by Yang *et al.* [2017] for the eastern United States. The first system resides in the rheologically transitional layer between the “pure” lithosphere and “pure” asthenosphere. This layer represents a gradual ~100 km thick transition from the lithosphere to the asthenosphere beneath ancient continents [Fischer *et al.*, 2010]. Simple shear in this layer associated with the relative movement between the lithosphere and asthenosphere can induce APM-parallel anisotropy. The second system is related to horizontally deflected flow in the asthenosphere along the edges of a region possessing relatively thick lithosphere. Such a flow system has been used to explain SWS measurements along the southern [Fouch *et al.*, 2000; Refayee *et al.*, 2014], western [Yang *et al.*, 2014; Refayee *et al.*, 2014], and eastern [Yang *et al.*, 2017] edges of the stable

North American continent. A detailed description of the model, together with a schematic diagram showing the corresponding flow fields, can be found in *Yang et al.* [2017].

In our study area, the existence of a region with anomalously thick lithosphere intersecting the central MRZ has been suggested by previous continental-scale surface wave tomographic studies [*Priestley et al.*, 2008; *Fishwick*, 2010], as well as by a recent receiver function study using the SAFARI data [*Reed et al.*, 2016]. The results of *Priestley et al.* [2008] reveal an area of thick lithosphere (where the thickness reaches 250 km) centered around the southern extent of the Victoria Microplate that thins progressively toward the south across the Tanganyika, Rukwa, and Malawi rift segments of the EARS. The largest lateral gradient of the lithospheric thickness is observed along an approximately E-W zone near the southern tip of Lake Malawi, where the lithospheric thickness is about 175 km. In contrast, *Fishwick* [2010] reported a “tongue-shaped” E-W trending zone of roughly 180–200 km thick lithosphere across the southern MRZ. These low-resolution (relative to the receiver function study using body waves recorded by local stations [*Reed et al.*, 2016]) surface wave tomographic observations are broadly consistent with an apparently shallower-than-normal 410 km discontinuity (Figure 9) in conjunction with a normal mantle transition zone (MTZ) thickness observed beneath northern Mozambique (Figure 9) [*Reed et al.*, 2016]. As argued in *Reed et al.* [2016], the high velocities in the upper mantle (i.e., above 410 km), which are associated with anomalously thick lithosphere, reduce the travel times of the *P*-to-*S* converted phases relative to the IASP91 reference Earth velocity model, thereby leading to an apparent (and thus, not real) uplift of both the 410 and 660 km MTZ boundary discontinuities. The E-W fast orientations observed in Mozambique align perfectly with the E-W strike of the southern edge of the anomalous region (Figure 9), the behavior of which is similar to edge-parallel fast orientations observed along the edges of the North American continent. Based upon the MTZ measurements from *Reed et al.* [2016] that are illustrated in Figure 9, the western edge of the anomalous region of lithospheric thicknesses is not as steep as the southern edge, and thus, its influence on mantle flow (and, therefore, on the splitting measurements) may not be as apparent. However, the approximately N-S ϕ measurements in eastern Zambia and western Malawi might reflect the influence of flow deflection along the broad western edge of the anomalous region, within which the MRZ has developed.

This model can explain both the single-layered and two-layered anisotropic structure. A single-layered structure is produced in the area with a relatively flat bottom of the lithosphere where edge-deflected flow is insignificant. It also develops when the deflected flow overprints fabrics in the lithosphere-asthenosphere transitional zone. This is likely the case for stations in Mozambique, eastern Zambia, and western Malawi. In addition, a net single-layer structure forms when the fast orientations of the two systems are parallel or orthogonal to each other. In the former case, the splitting time is the resultant sum of the individual layer anisotropies, while in the latter, the observed ϕ is that of the layer with the larger splitting time. On the other hand, if the two systems are at different depths and have nonparallel and nonorthogonal fast orientations, a two-layered structure is produced. The two-layered structure observed at the four stations in the northern MRZ (Figure 4) can be readily attributed to this model. While the nearly N-S oriented lower layer anisotropy is related to edge-deflected flow in the asthenosphere, the approximately NE-SW upper layer anisotropy roughly parallels the APM direction and thus may be related to simple shear developed within the lithosphere-asthenosphere transitional layer.

It should be mentioned that, as suggested by previous geodynamic modeling and SWS observational studies [*Fouch et al.*, 2000; *Yang et al.*, 2017], there is a 180° ambiguity in the direction of the flow systems. That is, relative to the lithosphere, an asthenospheric flow system moving toward the NE and being deflected eastward (northward) by the southern (western) edge of the area with thick lithosphere can create the observed splitting pattern in our study area. Meanwhile, a flow field toward the southwest can produce the same pattern.

4.5. Implications for Rift Initiation and Early Stage Development

The majority of the SWS measurements in the vicinity of both the MRZ and LRZ have a NE-SW orientation, which is similarly observed at most stations in southern Africa (Figure 1). This spatial consistency suggests the absence of a rift-parallel or rift-orthogonal small-scale flow system associated with rifting. It also implies the lack of an upwelling or downwelling flow system, which would be expected to reduce the splitting times and complicate the fast orientation pattern [*Ribe and Christensen*, 1994]. Although the results presented above are consistent with the notion that most continental rifts develop through lateral variations of lithospheric basal drag or resistive stresses along the edges of strong and thick continental blocks [e.g., *Yu et al.*, 2015], whether the magnitude of basal stress is sufficiently large to drive plate motion remains a debated topic

[Bird *et al.*, 2008; Ghosh and Holt, 2012; Stamps *et al.*, 2015]. A recent geodynamic modeling study [Stamps *et al.*, 2015] suggests that the magnitude of such basal stresses in the vicinity of the EARS is roughly an order of magnitude smaller than the deviatoric stresses associated with lithospheric gravitational potential energy gradients. The upper mantle origin of rifting beneath the MRZ inferred from these observations and previous geodynamic modeling studies [Stamps *et al.*, 2015] is consistent with the lack of a high-temperature mantle transition zone beneath the MRZ, and also with the recent realization that the MRZ is developing along the edge of a continental block with relatively thick lithosphere [Reed *et al.*, 2016]. Shear wave splitting and other geophysical measurements recently obtained in the vicinity of the Okavango and Rio Grande rifts are also consistent with this hypothesis [Yu *et al.*, 2015; Gao and Liu, 2016]. Moreover, numerical models of passive rifting in the EARS [Koptev *et al.*, 2015] suggest that torque-induced rotation of the continental lithosphere can achieve rupture absent high-magnitude far-field tensional stresses and without the presence of a viscous plume in the upper mantle, which may represent the geodynamic environment in the vicinity of the MRZ.

5. Conclusions

A number of deductions can be made based on the shear wave splitting measurements obtained from 34 SAFARI seismic stations situated along two profiles of ~1500 km length in the vicinity of the MRZ. First, with the exception of the area near the western boundary of the LRZ, the inconsistency between the observed fast orientations and the dominant trend of the major geological structures, as well as the resulting ~250 km depth of the center of the layer of anisotropy, suggest that fossil fabrics in the lithosphere are not a significant contributor to the observed anisotropy. Second, the large discrepancy between the observed anisotropy and that predicted by APM models involving a lithospheric net rotation component implies that the upper asthenosphere also has a westward net rotation with similar magnitude. Third, the similarity between the observed anisotropy and anisotropy predicted by no-net rotation APM models supports a model advocating the development of LPO in the transitional layer between the lithosphere and asthenosphere. Fourth, areas with fast orientations that are inconsistent with those predicted by NNR-APM models are mostly along the edges of an area with a relatively thick lithosphere, implying horizontal deflection of flow in the asthenosphere. Finally, this study provides additional evidence for the passive rifting model of the Malawi Rift Zone.

Acknowledgments

We offer thanks to the Incorporated Research Institutions for Seismology (IRIS) Data Management Center (DMC) for archiving and distributing the data used in the study, and the Portable Array Seismic Studies of the Continental Lithosphere (PASSCAL) Instrument Center for equipment and logistical support. Assistance provided by Shane Ingate of PASSCAL as well as by numerous government agencies and private citizens, especially Patrick R. N. Chindandali, Belarmino Massingue, Hassan Mdala, Daniel Mutamina, Gift Navilembo, Joseph Kayenta, and Francis Tchilongola, in Malawi, Mozambique, and Zambia during the field experiment is greatly appreciated. Constructive reviews from Associate Editor Hersh Gilbert and two anonymous reviewers significantly improved the clarity of the manuscript. All the data used in the study were obtained from the IRIS DMC (last accessed: August 2016). This study was supported by the U.S. National Science Foundation under grants 1009946 and 1460516 to S.G. and K.L. and by the University of Missouri Research Board.

References

- Ando, M., Y. Ishikawa, and H. Wada (1980), S-wave anisotropy in the upper mantle under a volcanic area in Japan, *Nature*, *286*, 43–46, doi:10.1038/286043a0.
- Argus, D. F., R. G. Gordon, and C. DeMets (2011), Geologically current motion of 56 plates relative to the no-net-rotation reference frame, *Geochem. Geophys. Geosyst.*, *12*, Q11001, doi:10.1029/2011GC003751.
- Bagley, B., and A. A. Nyblade (2013), Seismic anisotropy in eastern Africa, mantle flow, and the African superplume, *Geophys. Res. Lett.*, *40*, 1500–1505, doi:10.1002/grl.50315.
- Banks, N. L., K. A. Bardwell, and S. Musiwa (1995), Karoo Rift basins of the Luangwa Valley, Zambia, in *Hydrocarbon Habitat in Rift Basins*, *Geol. Soc. London Spec. Pub.*, vol. 80, edited by J. J. Lambiase, pp. 285–295.
- Barruol, G., and W. Ben Ismail (2001), Upper mantle anisotropy beneath the African IRIS and Geoscope stations, *Geophys. J. Int.*, *146*, 549–561.
- Becker, T. W., J. B. Kellogg, G. Ekstrom, and R. J. O'Connell (2003), Comparison of azimuthal seismic anisotropy from surface waves and finite strain from global mantle-circulation models, *Geophys. J. Int.*, *155*, 696–714, doi:10.1046/j.1365-246X.2003.02085.x.
- Becker, T. W., V. Schulte-Pelkum, D. K. Blackman, J. B. Kellogg, and R. J. O'Connell (2006), Mantle flow under the western United States from shear wave splitting, *Earth Planet. Sci. Lett.*, *247*, 235–251, doi:10.1016/j.epsl.2006.05.010.
- Bird, P., Z. Liu, and W. K. Rucker (2008), Stresses that drive the plates from below: Definitions, computational path, model optimization, and error analysis, *J. Geophys. Res.*, *113*, B11406, doi:10.1029/2007JB005460.
- Boyd, R., *et al.* (2010), The geology and geochemistry of the East African Orogen in northeastern Mozambique, *S. Afr. J. Geol.*, *113*, 87–129, doi:10.2113/gssajg.113.1.87.
- Calais, E., C. Ebinger, C. Hartnady, and J. M. Nocquet (2006), Kinematics of the East African Rift from GPS and earthquake slip vector data, in *The Afar Volcanic Province within the East African Rift System*, *Geol. Soc. London Spec. Pub.*, vol. 259, edited by G. Yirgu, C. J. Ebinger, and P. K. H. Maguire, pp. 9–22, doi:10.1144/GSL.SP.2006.259.01.03.
- Cherie, S. G., S. S. Gao, K. H. Liu, A. A. Elsheikh, F. Kong, C. A. Reed, and B. B. Yang (2016), Shear wave splitting analyses in Tian Shan: Geodynamic implications of complex seismic anisotropy, *Geochem. Geophys. Geosyst.*, *17*, 1975–1989, doi:10.1002/2016GC006269.
- Chorowicz, J. (2005), The East African rift system, *J. Afr. Earth Sci.*, *43*, 379–410, doi:10.1016/j.jafrearsci.2005.07.019.
- Conrad, C. P., and M. D. Behn (2010), Constraints on lithosphere net rotation and asthenospheric viscosity from global mantle flow models and seismic anisotropy, *Geochem. Geophys. Geosyst.*, *11*, Q05W05, doi:10.1029/2009GC002970.
- Craig, T. J., J. A. Jackson, K. Priestley, and D. McKenzie (2011), Earthquake distribution patterns in Africa: Their relationship to variations in lithospheric and geological structure, and their rheological implications, *Geophys. J. Int.*, *185*, 403–434, doi:10.1111/j.1365-246X.2011.04950.x.
- Delvaux, D., K. Levi, R. Kajara, and J. Sarota (1992), Cenozoic paleostress and kinematic evolution of the Rukwa-North Malawi rift valley (East African Rift System), *Bull. Centres Rech. Explor. Prod. Elf Aquitaine*, *16*, 383–406.
- DeMets, C., R. G. Gordon, D. F. Argus, and S. Stein (1994), Effect of recent revisions to the geomagnetic reversal time scale on estimates of current plate motions, *Geophys. Res. Lett.*, *21*, 2191–2194.

- Ebinger, C. J., A. L. Deino, R. E. Drake, and A. L. Tesha (1989), Chronology of volcanism and rift basin propagation: Rungwe Volcanic Province, East Africa, *J. Geophys. Res.*, *94*, 15,785–15,803.
- Ebinger, C. J., A. L. Deino, A. L. Tesha, T. Becker, and U. Ring (1993), Tectonic controls on rift basin morphology: Evolution of the northern Malawi (Nyasa) rift, *J. Geophys. Res.*, *98*, 17,821–17,836.
- Elsheikh, A. A., S. S. Gao, K. H. Liu, A. A. Mohamed, Y. Yu, and R. E. Fat-Helbary (2014), Seismic anisotropy and subduction-induced mantle fabrics beneath the Arabian and Nubian Plates adjacent to the Red Sea, *Geophys. Res. Lett.*, *41*, 2376–2381, doi:10.1002/2014GL059536.
- Fischer, K. M., H. A. Ford, D. L. Abt, and C. A. Rychert (2010), The lithosphere-asthenosphere boundary, *Annu. Rev. Earth Planet Sci.*, *38*, 551–575, doi:10.1146/annurev-earth-040809-152438.
- Fishwick, S. (2010), Surface wave tomography: Imaging of the lithosphere-asthenosphere boundary beneath central and southern Africa, *Lithos*, *120*, 63–73, doi:10.1016/j.lithos.2010.05.011.
- Fouch, M. J., K. M. Fischer, E. M. Parmentier, M. E. Wysession, and T. J. Clarke (2000), Shear wave splitting, continental keels, and patterns of mantle flow, *J. Geophys. Res.*, *105*, 6255–6275.
- Fritz, H., et al. (2013), Orogen styles in the East African Orogen: A review of the Neoproterozoic to Cambrian tectonic evolution, *J. Afr. Earth Sci.*, *86*, 65–106, doi:10.1016/j.jafrearsci.2013.06.004.
- Gao, S. S., and K. H. Liu (2009), Significant seismic anisotropy beneath the southern Lhasa Terrane, Tibetan Plateau, *Geochem. Geophys. Geophys.*, *10*, Q02008, doi:10.1029/2008GC002227.
- Gao, S. S., and K. H. Liu (2012), AnisDep: A FORTRAN program for the estimation of the depth of anisotropy using spatial coherency of shear-wave splitting parameters, *Comp. Geosci.*, *49*, 330–333, doi:10.1016/j.cageo.2012.01.020.
- Gao, S. S., and K. H. Liu (2016), Rifting initiation through lateral variations of lithospheric basal stress beneath preexisting zones of weakness, Paper No. 229-1, vol. 48, Geol. Soc. of Am. Annual Meeting, Denver, Colo.
- Gao, S., P. M. Davis, H. Liu, P. D. Slack, Y. A. Zorin, V. V. Mordvinova, V. M. Kozhevnikov, and R. P. Meyer (1994), Seismic anisotropy and mantle flow beneath the Baikal rift zone, *Nature*, *371*, 149–151.
- Gao, S., P. M. Davis, H. Liu, P. D. Slack, A. W. Rigor, Y. A. Zorin, V. V. Mordvinova, V. M. Kozhevnikov, and N. A. Logatchev (1997), SKS splitting beneath continental rift zones, *J. Geophys. Res.*, *102*, 22,781–22,797, doi:10.1029/97JB01858.
- Gao, S. S., K. H. Liu, and M. G. Abdelsalam (2010), Seismic anisotropy beneath the Afar Depression and adjacent areas: Implications for mantle flow, *J. Geophys. Res.*, *115*, B12330, doi:10.1029/2009JB007141.
- Gao, S. S., et al. (2013), Seismic arrays to study African rift initiation, *Eos Trans. AGU*, *94*, 213, doi:10.1002/2013EO240002.
- Ghosh, A., and W. E. Holt (2012), Plate motions and stresses from global dynamic models, *Science*, *335*, 838–843, doi:10.1126/science.1214209.
- Gripp, A. E., and R. G. Gordon (2002), Young tracks of hotspots and current plate velocities, *Geophys. J. Int.*, *150*, 321–361, doi:10.1046/j.1365-246X.2002.01627.x.
- Hammond, J. O. S., J. M. Kendall, J. Wookey, G. W. Stuart, D. Keir, and A. Ayele (2014), Differentiating flow, melt, or fossil anisotropy beneath Ethiopia, *Geochem. Geophys. Geosyst.*, *15*, 1878–1894, doi:10.1002/2013GC005185.
- Hanson, R. E. (2003), Proterozoic geochronology and tectonic evolution of southern Africa, *Geol. Soc. London Spec. Pub.*, *206*, 427–463.
- Huerta, A. D., A. A. Nyblade, and A. M. Reusch (2009), Mantle transition zone structure beneath Kenya and Tanzania: More evidence for a deep-seated thermal upwelling in the mantle, *Geophys. J. Int.*, *177*, 1249–1255, doi:10.1111/j.1365-246X.2009.04092.x.
- Koptev, A., E. Calais, E. Burov, S. Leroy, and T. Gerya (2015), Dual continental rift systems generated by plume-lithosphere interaction, *Nat. Geosci.*, *8*, 388–392, doi:10.1038/NGEO2401.
- Laó-Dávila, D. A., H. S. Al-Salmi, M. G. Abdelsalam, and E. A. Atekwana (2015), Hierarchical segmentation of the Malawi Rift: The influence of inherited heterogeneity and kinematics in the evolution of continental rifts, *Tectonics*, *34*, 2399–2417, doi:10.1002/2015TC003953.
- Lemnifi, A., K. H. Liu, S. S. Gao, C. A. Reed, A. Elsheikh, Y. Yu, and A. Elmélade (2015), Azimuthal anisotropy beneath north central Africa from shear wave splitting analyses, *Geochem. Geophys. Geosyst.*, *16*, 1105–1114, doi:10.1002/2014GC005706.
- Liu, K. H., and S. S. Gao (2011), Estimation of the depth of anisotropy using spatial coherency of shear-wave splitting parameters, *Bull. Seismol. Soc. Am.*, *101*, 2153–2161, doi:10.1785/0120100258.
- Liu, K. H., and S. S. Gao (2013), Making reliable shear-wave splitting measurements, *Bull. Seismol. Soc. Am.*, *103*(5), 2680–2693, doi:10.1785/0120120355.
- Liu, K. H., S. S. Gao, Y. Gao, and J. Wu (2008), Shear wave splitting and mantle flow associated with the deflected Pacific slab beneath northeast Asia, *J. Geophys. Res.*, *113*, B01305, doi:10.1029/2007JB005178.
- Liu, K. H., A. Elsheikh, A. Lemnifi, U. Purevsuren, M. Ray, H. Refayee, B. B. Yang, Y. Yu, and S. S. Gao (2014), A uniform database of teleseismic shear wave splitting measurements for the western and central United States, *Geochem. Geophys. Geosyst.*, *15*, 2075–2085, doi:10.1002/2014GC005267.
- Long, M. D., and P. G. Silver (2009), Shear wave splitting and mantle anisotropy: Measurements, interpretations, and new directions, *Surv. Geophys.*, *30*, 407–461, doi:10.1007/s10712-009-9075-1.
- Priestley, K., D. McKenzie, E. Debayle, and S. Pilidou (2008), The African upper mantle and its relationship to tectonics and surface geology, *Geophys. J. Int.*, *175*, 1108–1126, doi:10.1111/j.1365-246X.2008.03951.x.
- Reed, C. A., K. H. Liu, P. R. N. Chindandali, B. Massingue, H. Mdala, D. Mutamina, Y. Yu, and S. S. Gao (2016), Passive rifting of thick lithosphere in the southern East African Rift: Evidence from mantle transition zone discontinuity topography, *J. Geophys. Res.*, *121*, 8068–8079, doi:10.1002/2016JB013131.
- Refayee, H. A., B. B. Yang, K. H. Liu, and S. S. Gao (2014), Mantle flow and lithosphere-asthenosphere coupling beneath the southwestern edge of the North American Craton: Constraints from shear-wave splitting measurements, *Earth Planet. Sci. Lett.*, *402*, 209–220, doi:10.1016/j.epsl.2013.01.031.
- Ribe, N. M., and U. R. Christensen (1994), Three-dimensional modeling of plume-lithosphere interaction, *J. Geophys. Res.*, *99*, 669–682.
- Saria, E., E. Calais, D. S. Stamps, D. Delvaux, and C. J. H. Hartnady (2014), Present-day kinematics of the East African Rift, *J. Geophys. Res. Solid Earth*, *119*, 3584–3600, doi:10.1002/2013JB010901.
- Savage, M. K. (1999), Seismic anisotropy and mantle deformation: What have we learned from shear wave splitting?, *Rev. Geophys.*, *37*, 65–106, doi:10.1029/98RG02075.
- Shillington, D. J., et al. (2016), Acquisition of a unique onshore/offshore geophysical and geochemical dataset in the northern Malawi (Nyasa) Rift, *Seismol. Res. Lett.*, *87*, 1406–1416, doi:10.1785/0220160112.
- Silver, P. G. (1996), Seismic anisotropy beneath the continents: Probing the depths of geology, *Annu. Rev. Earth Planet. Sci.*, *24*, 385–432.
- Silver, P. G., and W. W. Chan (1991), Shear wave splitting and subcontinental mantle deformation, *J. Geophys. Res.*, *96*, 16,429–16,454.
- Silver, P. G., and M. Savage (1994), The interpretation of shear-wave splitting parameters in the presence of two anisotropic layers, *Geophys. J. Int.*, *119*, 949–963.

- Silver, P. G., S. S. Gao, K. H. Liu, and the Kaapvaal Seismic Group (2001), Mantle deformation beneath southern Africa, *Geophys. Res. Lett.*, *28*, 2493–2496.
- Stamps, D. S., E. Calais, E. Saria, C. Hartnady, J.-M. Nocquet, C. J. Ebinger, and R. M. Fernandes (2008), A kinematic model for the East African Rift, *Geophys. Res. Lett.*, *35*, L05304, doi:10.1029/2007GL032781.
- Stamps, D. S., L. M. Flesch, E. Calais, and A. Ghosh (2014), Current kinematics and dynamics of Africa and the East African Rift System, *J. Geophys. Res. Solid Earth*, *119*, 5161–5186, doi:10.1002/2013JB010717.
- Stamps, D. S., G. Iaffaldano, and E. Calais (2015), Role of mantle flow in Nubia-Somalia plate divergence, *Geophys. Res. Lett.*, *42*, 290–296, doi:10.1002/2014GL062515.
- Tepp, G. (2016), Seismic analysis of magmatism in the Galápagos Archipelago and East Africa, PhD dissertation, 162 pp., Univ. of Rochester, Rochester, New York.
- Tommasi, A., and A. Vauchez (2001), Continental rifting parallel to ancient collisional belts: An effect of the mechanical anisotropy of the lithospheric mantle, *Earth Planet. Sci. Lett.*, *185*, 199–210.
- Tommasi, A., A. Vauchez, and R. Russo (1996), Seismic anisotropy in ocean basins: Resistive drag of the sublithospheric mantle?, *Geophys. Res. Lett.*, *23*, 2991–2994, doi:10.1029/96GL02891.
- Walker, K. T., A. A. Nyblade, S. L. Klemperer, G. H. R. Bokelmann, and T. J. Owens (2004), On the relationship between extension and anisotropy: Constraints from shear wave splitting across the East African Plateau, *J. Geophys. Res.*, *109*, B08302, doi:10.1029/2003JB002866.
- Yang, B. B., S. S. Gao, K. H. Liu, A. A. Elsheikh, A. A. Lemnifi, H. A. Refayee, and Y. Yu (2014), Seismic anisotropy and mantle flow beneath the northern Great Plains of North America, *J. Geophys. Res. Solid Earth*, *119*, 1971–1985, doi:10.1002/2013JB010561.
- Yang, B. B., Y. Liu, H. Dahm, K. H. Liu, and S. S. Gao (2017), Seismic azimuthal anisotropy beneath the eastern United States and its geodynamic implications, *Geophys. Res. Lett.*, *44*, 2670–2678, doi:10.1002/2016GL071227.
- Yu, Y., S. S. Gao, M. Moidaki, C. A. Reed, and K. H. Liu (2015), Seismic anisotropy beneath the incipient Okavango rift: Implications for rifting initiation, *Earth Planet. Sci. Lett.*, *430*, 1–8, doi:10.1016/j.epsl.2015.08.009.
- Zhang, S., and S.-I. Karato (1995), Lattice preferred orientation of olivine aggregates deformed in simple shear, *Nature*, *375*, 774–777, doi:10.1038/375774a0.